GA–A24131

CORRELATION OF H–MODE BARRIER WIDTH AND NEUTRAL PENETRATION LENGTH

by
R.J. GROEBNER, M.A. MAHDAVI, A.W. LEONARD, T.H. OSBORNE,
N.S. WOLF, G.D. PORTER, P.C. STANGEBY, N.H. BROOKS,
R.J. COLCHIN, W.W. HEIDBRINK, T.C. LUCE, G.R. McKEE,
L.W. OWEN, G. WANG, and D.G. WHYTE

SEPTEMBER 2002

DISCLAIMER

This report was prepared as an account of work sponsored by an agency of the United States Government. Neither the United States Government nor any agency thereof, nor any of their employees, makes any warranty, express or implied, or assumes any legal liability or responsibility for the accuracy, completeness, or usefulness of any information, apparatus, product, or process disclosed, or represents that its use would not infringe privately owned rights. Reference herein to any specific commercial product, process, or service by trade name, trademark, manufacturer, or otherwise, does not necessarily constitute or imply its endorsement, recommendation, or favoring by the United States Government or any agency thereof. The views and opinions of authors expressed herein do not necessarily state or reflect those of the United States Government or any agency thereof.

GA–A24131

CORRELATION OF H–MODE BARRIER WIDTH AND NEUTRAL PENETRATION LENGTH

by

R.J. GROEBNER, M.A. MAHDAVI, A.W. LEONARD, T.H. OSBORNE, N.S. WOLF,* G.D. PORTER,* P.C. STANGEBY,† N.H. BROOKS, R.J. COLCHIN,‡ W.W. HEIDBRINK,◊ T.C. LUCE, G.R. McKEE,Δ L.W. OWEN,‡ G. WANG,£ and D.G. WHYTE+#

This is a preprint of a paper to be presented at the 19th IAEA Fusion Energy Conference, October 14–19, 2002, Lyon, France, and to be published in *Nuclear Fusion.*

*Lawrence Livermore National Laboratory, Livermore, California.
†University of Toronto, Toronto, Canada.
‡Oak Ridge National Laboratory, Oak Ridge, Tennessee.
◊University of California, Irvine, California.
ΔUniversity of Wisconsin-Madison, Madison Wisconsin.
£University of California, Los Angeles, California.
+University of California, San Diego, La Jolla, California.
#Present Address: University of Wisconsin-Madison, Madison Wisconsin.

Work supported by
U.S. Department of Energy under
Contracts DE-AC03-99ER54463, W-7405-ENG-48, DE-AC05-00OR22725, SC-G903402, and Grants DE-FG03-96ER54373, DE-FG03-01ER54615, and DE-FG03-95ER54294

GENERAL ATOMICS PROJECT 30033
SEPTEMBER 2002

ABSTRACT

Pedestal studies in DIII–D find a good correlation between the width of the region of steep gradient in the H–mode density and the neutral penetration length. These results are obtained by comparing experimental density profiles to the predictions of an analytic model for the profile, obtained from the particle continuity equations for electrons and deuterium atoms. In its range of validity (edge temperature between 40–500 eV), the analytic model quantitatively predicts the observed decrease of the width as the pedestal density increases, the observed strong increase of the gradient of the density as the pedestal density increases and the observation that L–mode and H–mode profiles with the same pedestal density have very similar shapes. The width of the density barrier, measured from the edge of the electron temperature barrier, is the lower limit for the observed width of the temperature barrier. These results support the hypothesis that particle fueling provides a dominant control for the size of the H–mode transport barrier.

1. INTRODUCTION

Experimental observations and theoretical modeling show that the height of the H–mode pedestal has a large impact on tokamak performance [1-3]. Therefore, uncertainties in the scaling of the pedestal lead to significant uncertainties in the performance of next-step machines. For these reasons, obtaining a scaling for the height of the H–mode pedestal has been an important topic of fusion research for the last several years. In contemporary understanding, this issue is sub-divided into two problems, understanding the limitations on the pressure gradient imposed by MHD stability [4] and understanding the scaling of the width of the H–mode barrier, the region of good edge confinement. This paper examines the physics of the width of the edge transport barrier.

Self-consistent transport theories, based on the hypothesis that shear in the E×B velocity stabilizes turbulence, predict that transport barriers are formed by sufficiently large sources of heat, particles or momentum [5,6]. These theories embody solutions of the transport equations, which the plasma must obey, and may be viewed as containing the minimal physics that is present in the structure of transport barriers. In the Hinton-Staebler model [5], developed for the H–mode transport barrier, the shearing rate of the turbulence depends on gradients of the density and pressure with $\Omega_{ExB} \sim \frac{dn_i}{dr}\frac{dp_i}{dr}$ where n_i and p_i are the ion density and pressure, respectively, and the gradients are taken in the direction perpendicular to the magnetic field. This expression predicts that the barrier requires a sufficient gradient in the ion density. Furthermore, the theory predicts that the width of the transport barrier is determined primarily by the width of the edge particle source with an additional weak dependence on the heat flux from the core plasma.

This paper presents results of studies in the DIII–D tokamak to address two basic questions posed by the Hinton-Staebler model. First, is the steep gradient region of the edge density profile (density step) produced by the fueling neutrals? A number of studies in DIII–D strongly indicate that the answer is "yes". These studies are based primarily on the use of an analytic model (Section 2) to study various features of the edge density profile. With standard assumptions about the model parameters, the model is quantitatively consistent with the measured widths (Section 3.2) and gradients (Section 3.3) of the edge density profile over a wide range of densities. Moreover, it is found that L–mode and H–mode density profiles with similar values of the pedestal density have quite similar shapes (Section 3.4). Benchmarking studies (Section 3.5) show that the simple analytic model compares favorably with a much more sophisticated edge modeling code in the regime where charge exchange neutrals are expected to dominate edge fueling. Sensitivity studies (Section 3.6) show that a square-well form for the diffusion

coefficient modifies the details but not the general conclusions as obtained from the basic model, which uses a spatially constant diffusivity. The most important known limitation of the model is that it does not describe trends that have sometimes been observed at high edge temperature (Section 3.7). These trends are observed in a region where the model is not expected to apply and potentially could be explained by a more sophisticated model. In sum, these studies lead to the conclusion that atomic as well as plasma physics plays a role in determining the shape of the edge electron density profile.

A second question studied here is: Is the width of the H–mode transport barrier approximately equal to the width of the steep gradient region of the density profile? This question is studied by examining the width of the barrier in the electron temperature as compared to the width of the density barrier, with both widths being measured from the foot of the electron temperature barrier. It is found that this ratio is close to but on average slightly greater than one (Section 4). These results are consistent with the density step, and therefore the fueling source, providing a lower limit for the transport barrier width. Thus, the experimental findings here are consistent with the basic assertions of the Hinton-Staebler model.

2. ANALYTICAL MODEL FOR DENSITY PROFILE

An analytical model has been developed to study the interplay of atomic physics and plasma physics in forming the edge electron density profile. The electron density is used here as a proxy for the ion density because measurements of density are readily available for the electrons. The formulation used here is based on the work of Wagner, Lackner and Engelhardt [7,8] and the derivation is discussed in detail elsewhere [9–13]. In brief, an equation for the edge electron density profile in slab geometry is obtained from a self-consistent solution of the particle continuity equations for the electrons and the deuterium atoms, with impurities ignored. The flux of electrons Γ_e is assumed to have the form $\Gamma_e = -D dn_e/dx$, where D is the particle diffusion coefficient and x is a spatial coordinate perpendicular to the magnetic surface. The flux of deuterons Γ_n is assumed to have the form $\Gamma_n = n_n V_n$, where n_n is the neutral density and V_n is the inward neutral velocity perpendicular to the magnetic surface. The diffusion coefficient and neutral velocity are assumed to be constant in space.

Recently, this model has been extended by Mahdavi [9,13] to allow for different diffusion coefficients on the open and closed field lines and for a neutral source that is localized in the poloidal direction. Inside the separatrix, the resulting profile for n_e as measured along x is

$$n_e(x) = n_{e,ped} \tanh\left[C - \left(\sigma_i V_e / 2V_n\right) n_{e,ped} E\, x\right] \quad , \tag{1}$$

with $n_{e,ped}$ being the pedestal density as $x \rightarrow -\infty$, σ_i being the ionization cross section, V_e being the electron thermal velocity and E being the ratio of the distances between two flux surfaces at the poloidal angle of the particle source and at the poloidal angle θ_m where the measurement is made. The geometric parameter E is in some sense a measure of the efficiency of fueling at a given poloidal location. For typical diverted discharges in DIII–D, the value of E for fueling in the vicinity of the X–point is about an order of magnitude larger than for fueling at the outside midplane. Thus, fueling in the X–point is not favorable for producing large widths in the density profile. Ionization in the scrape-off layer (SOL) is neglected. All ionization occurs inside the LCFS with particles diffusing onto the open field lines, where they are rapidly transported by parallel flow to the divertor and lost. Thus, the SOL physics acts as a sink of particles and helps to set up the gradient of the density profile at and inside the LCFS. This SOL physics is modeled by assuming that n_e has the source-free Yokomizo solution [14]

$$n_e(x) = n_{e,sep} \exp\left(-x / \sqrt{D_s \tau_{\|}}\right) \quad , \tag{2}$$

where $n_{e,sep}$ is the electron density at the separatrix (LCFS), D_s is the diffusion coefficient in the SOL and $\tau_{\|}$ is the average particle lifetime for parallel flow to the divertor plates. The integration constant C in Eq. (1), obtained by continuity of n_e and its first derivative at x=0, is

$$C = 0.5\,\sinh^{-1}(U), \quad U = \left[\sqrt{D_s \tau_{\|}}\,\sigma_i V_e / V_n\right] E n_{e,ped}\, D_c / D_s \quad , \tag{3}$$

where D_c is the diffusion coefficient in the core. Equation (1) can be written as

$$n_e(x) = n_{e,ped} \tanh\left[C - x/\Delta_{ne}\right] \quad , \tag{4}$$

with

$$\Delta_{ne} = 2V_n \Big/ \left(\sigma_i V_e E n_{e,ped}\right) \quad , \tag{5}$$

The separatrix density has a finite value as given by

$$n_{e,sep} = n_{e,ped} \tanh[C] \quad , \tag{6}$$

In the fueling region inside the core, the neutral density profile is given by

$$n_n(x) = (D_c / V_n)(n_{e,ped} / \Delta_{ne}) \operatorname{sech}^2[C - x/\Delta_{ne}]. \quad . \tag{7}$$

Inspection of Eqs. (4) and (6) shows that Δ_{ne} is the characteristic attenuation length for both the rise of the electron density and the penetration of the neutrals inside the LCFS. Thus, the characteristic width of the steep gradient region of the electron density is approximately equal to the ionization length for the neutrals. Under the assumption that C is small (small density at the LCFS), Eq. (7) can be evaluated at the LCFS and re-written to provide an alternate expression for $n_{e,ped}$:

$$n_{e,ped} \approx V_n \sqrt{2 n_n(0) / D_c \sigma_i V_e E} \quad , \tag{8}$$

where $n_n(0)$ is the neutral density at the LCFS in the fueling region.

There are several important physics implications of the model shown here. Equation (8) shows that $n_{e,ped}$ is fundamentally determined by a combination of plasma physics (D_c, V_e), atomic physics ($V_n, n_n(0), \sigma_i$) and geometry (E). In fact V_n and σ_i are also determined partially by the plasma temperature, so these parameters are set by an inseparable combination of plasma and atomic physics. Equation (8) also shows that $n_{e,ped} \propto \sqrt{n_n(0)/D_c}$ and thus is determined by

a competition between neutral physics and plasma transport. A profile with a given $n_{e,ped}$ can be produced with very different values of the diffusion coefficient, so long as the neutral density is adjusted appropriately to maintain the necessary ratio of $n_n(0)/D_c$. Nevertheless, Eqs. (4) and (5) imply that the characteristic scale length inside the LCFS for a profile with given $n_{e,ped}$ is independent of the diffusion coefficient, no matter what its value is. However, particle transport both inside and outside the LCFS helps to set the separatrix density, which depends on C [Eq. (6)] which in turn depends on $D_c/\sqrt{D_s}$ [Eq. (3)]. Thus, for profiles with the same $n_{e,ped}$, differences in particle transport will be reflected primarily in the value of $n_{e,sep}$.

One of the major limitations of this model is that the possibility for neutral diffusion due to multiple charge exchange events is ignored due to the intractability of this physics in an analytic model. The omission of this physics restricts the applicability of the model to edge temperatures in the approximate range 40–500 eV, in which the ionization rate is comparable to the charge exchange rate.

3. COMPARISON OF DATA TO ANALYTICAL MODEL

The analytic model discussed in the previous section can be used to make predictions, useful for comparison with data, and these will be discussed here.

3.1. Evaluating the analytical model

For a given value of $n_{e,ped}$, the model predicts that the density inboard of the LCFS depends on five parameters: D_c, D_s, E, V_n and T_e (used to compute σ_i and V_e). As will be discussed where appropriate, the model is sensitive to some parameters and not very sensitive to others. However, these parameters must be assigned values in order to evaluate the model and the assignment is performed as follows. Values for the diffusion coefficients are obtained from typical results of edge modeling analysis. The nominal values of D_s and D_c are taken as 0.14 and 0.4 m^2/s, respectively. The nominal value of T_e is taken as 75 eV, a representative value at the LCFS. The geometric factor E will ultimately be chosen to give best consistency with the data, as discussed later. However, modeling of the pedestal and SOL density profile, as performed with the sophisticated edge modeling code UEDGE [15] provides insight as to what values might be expected. For the diverted discharges typical of DIII–D, UEDGE predicts that most of the fueling occurs in a distributed region in the vicinity of the X–point; the average value of E for fueling in that region with measurements being made at the outboard midplane is in the range 6–8.

The final parameter required to evaluate the model is the neutral velocity V_n at the LCFS. The physics of the travel of neutrals through the SOL plasma from the divertor plate and walls to the LCFS may be tortuous and the energy distribution of the neutrals arriving at the LCFS may be complex. However, to lowest order it can be assumed that these neutrals have two distributions: those which are Frank-Condon neutrals with temperatures of ~ 3 eV and those which have charge-exchanged with plasma ions and have approximately the temperature of the ions at the LCFS. The ion temperature is taken as twice the electron temperature. At sufficiently low plasma densities, neutrals at the LCFS will be predominantly Frank-Condon neutrals and at sufficiently high densities they will be predominantly charge-exchange neutrals. A simple fluid model has been developed to compute the ratio of the density of charge-exchange neutrals to Frank-Condon neutrals and the V_n is computed as the average inward velocity of the resulting neutral populations [13]. A slight correction to the neutral velocity is performed to account for the fact that there will be about one charge exchange event in the plasma per ionization event and as a result, the average neutral penetration length is slightly reduced [13].

3.2. Scaling of width of density profile

Equation (5) shows that the width parameter Δ_{ne} depends on both atomic physics and plasma physics parameters. However, for fixed temperatures and fixed fueling location, Eq. (5) predicts that $\Delta_{ne} \sim 1/n_{e,ped}$. Experimental data can be used to test this prediction. Moreover, with an appropriate estimate for the geometric factor E, a quantitative comparison can be made between theory and experiment. Widths of experimental density profiles W_{ex} are obtained by fitting functions with a hyperbolic tangent shape (plus appropriate linear terms) [16] to electron density profiles obtained with the DIII–D multi-pulse Thomson scattering system [17]. A complication in comparing these widths with the model is that W_{ex} includes not only Δ_{ne} but also that part of the width that lies outside the LCFS. In contrast, the width parameter Δ_{ne} in the model lies entirely inside the LCFS. Thus, W_{ex} is not necessarily a good approximation of Δ_{ne}. In principle, it is desirable to compute an experimental value for Δ_{ne} by subtracting that part of the width which lies outside the LCFS from the experimental measurement of W_{ex}. In practice, this approach requires the determination of the location of the LCFS from an equilbrium construction. This determination has potential errors of up to 1 cm, which are comparable to the widths being measured. Thus, computing an experimental value for Δ_{ne} tends to add scatter to the data and somewhat obscure trends which are more obvious when the entire experimental width W_{ex} is plotted. Because of this difficulty, a theoretical width W_{th} has been defined to emulate the experimental width W_{ex}. W_{th} is defined as the distance over which the model density profile varies from 88% of $n_{e,ped}$ to 12% of $n_{e,ped}$. This definition emulates the width in the *tanh* form, used to determine W_{ex}, under the assumption that the constant density term in the experimental fit is small, an assumption which is usually well met.

Figure 1 shows that the widths W_{th} computed from the model compare well with W_{ex} from experimental data. The data are obtained from systematic scans of $n_{e,ped}$ in which the plasma shape was maintained approximately constant, large plasma-wall gaps were maintained to ensure that fueling always occurred from the same poloidal location, gas fueling was used to increase the density and cryopumping was used to reduce the density. The data are averaged over 50–300 ms in order to reduce scatter, presumably due to turbulence, and data with ELMs are eliminated from the plot. Edge temperatures were sufficiently low so that the model should be applicable. For the evaluation of W_{th}, the free parameters were given the values as discussed in Section 3.1. Evaluation of W_{th} generally requires computation of the density profile in the SOL with the aid of Eq. (2). For this purpose, the average particle lifetime in the SOL $\tau_{||}$ is given a value representative of typical discharges used in the study. Results are quite insensitive to the exact value of $\tau_{||}$. The geometric parameter E was adjusted to give a "best" fit of the model to the data. With the experimental widths mapped to the outer midplane, a value of E of 7 was

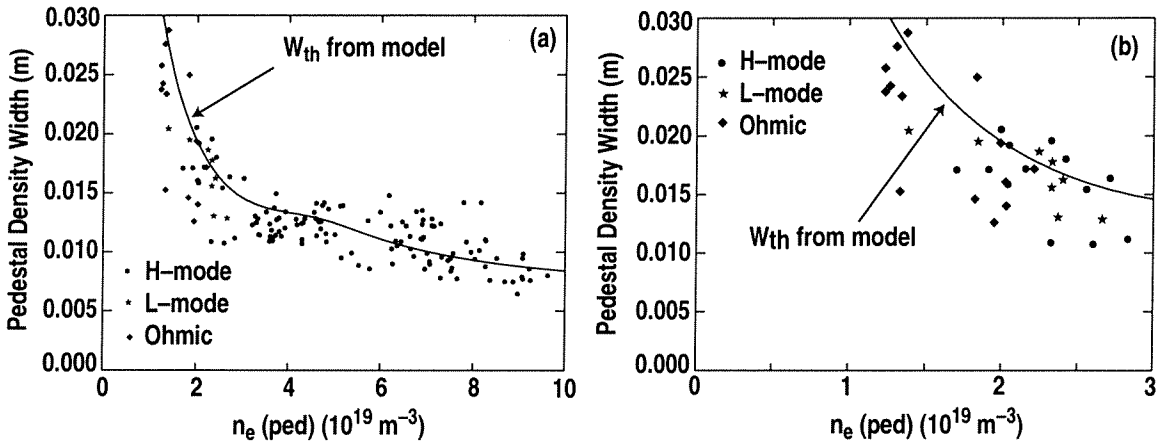

Fig. 1. Widths of edge density profile, normalized to outboard midplane, versus pedestal density. Experimental widths from H–mode (circles), L–mode (stars) and Ohmic (triangles) discharges. Solid curve is theoretical width W_{th} with parameters at nominal values with Frank-Condon neutrals included. (a) Data plotted over full density range; (b) blowup of data at low density, showing more clearly the overlap of Ohmic, L–mode and H–mode data.

chosen and this is well in line with expectations based on UEDGE modeling, as discussed previously. The experimental widths show a systematic decrease as the pedestal density increases, a qualitative behavior expected from Eq. (5). One feature of the data is that there is a flattening of this trend for $n_{e,ped}$ in the range $2-4\times10^{19}m^{-3}$. This is understood as being due to the crossover between the influence of Frank-Condon neutrals at low densities and charge exchange neutrals at high densities.

Data from Ohmic, L–mode and H–mode discharges are shown in Fig. 1. For the range of $n_{e,ped}$ in which L–mode and H–mode data are simultaneously obtained, about $2-3\times10^{19}m^{-3}$, the widths are virtually the same, despite the fact that the edge transport is markedly different for the two regimes. These data provide strong evidence that the width of the H–mode density barrier cannot be understood purely in terms of the diffusion coefficient. The model used here, which includes self-consistently the particle source, is consistent with these results. In particular, Eq. (5) shows that the ratio of the width inside the LCFS to the pedestal density is independent of particle diffusion, under the approximations used here. Some dependence of the total experimental width on diffusion is introduced by Eq. (2), which accounts for the density in the SOL. However, this dependence is very weak. Sensitivity studies have shown that D_c or D_s must be increased by about an order of magnitude before a significant change is observed in the model prediction. Even then, the changes in the model width are modest. The model is affected much more dramatically by changes in the fueling location (E) or by a change in the ratio of neutral velocity to electron thermal velocity.

3.3. Scaling of gradient of density profile

The analytic model can also be used to compute the maximum gradient of the edge density profile and the results can be compared to data. The results compare very favorably as will be shown. From Eq. (4), it can be shown that the gradient inboard of the LCFS is

$$\partial n_e(x)/\partial x = -(n_{e,ped}/\Delta_{ne})\mathrm{sech}^2[C - x/\Delta_{ne}]. \quad . \tag{9}$$

The argument of the sech is always positive inboard of the LCFS, and thus, the gradient reaches its maximum value at the LCFS. For small C, obtained when the separatrix density is small relative to the pedestal density, the maximum gradient is approximately $\max(-\nabla n_e)_{th} = n_{e,ped}/\Delta_{ne}$. Thus, the gradient is predicted to vary approximately as $n_{e,ped}{}^2$. The maximum gradient from the experiment $\max(-\nabla n_e)_{ex}$ is easily calculated from fits of the *tanh* function to the data. A comparison of the data and the model prediction is shown in Fig. 2, which use the same experimental data set and the same model parameters as used in Fig. 1. The gradients are mapped to the outboard midplane. The model, which includes Frank-Condon neutrals, shows good agreement with the data.

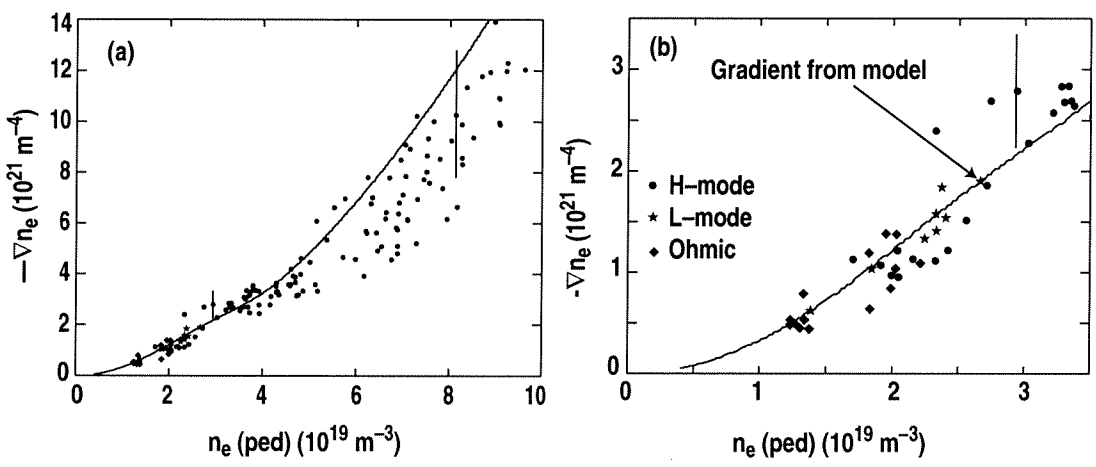

Fig. 2. Maximum gradients of edge density profile, normalized to outboard midplane, versus pedestal density. Experimental gradients from H–mode (circles), L–mode (stars) and Ohmic (triangles) discharges. Curve is model gradient with nominal parameters. Vertical bars show approximate range of data prior to averaging. (a) Data plotted over full density range; (b) blowup of data at low density, showing more clearly the overlap of Ohmic, L–mode and H–mode data.

As in the case of the widths, the experimental gradients for L–mode and H–mode data overlap to a high degree, occurring in the range $2-3\times10^{19}m^{-3}$, despite the fact that transport is very different for the H–mode and L–mode data. The analytic model shows how this is possible. The gradient at the LCFS depends on the diffusion coefficients only through the parameter C in

Eq. (9). Since transport does not enter directly into the width parameter Δ_{ne}, transport can only affect the gradient (at fixed $n_{e,ped}$) by increasing C and therefore the value of the density at the LCFS. As will be shown later, a large increase of both D_c and D_s results in a very modest change in the gradient. Thus, it is quite plausible that very similar gradients can be achieved despite rather different transport coefficients.

3.4. Comparison of L–mode and H–mode profiles

Another way of illustrating the prediction of Eq. (5), that for fixed $n_{e,ped}$ the width inboard of the LCFS is independent of diffusion, is to compare density profiles of L–mode and H–mode discharges with the same $n_{e,ped}$. In general, it is difficult to do this because H–mode discharges tend to operate at much higher values of $n_{e,ped}$ than L-mode discharges. However, for an H–mode discharge with strong cryopumping to reduce the density and an L–mode discharge with strong gas-puffing to increase the density, L–mode and H–mode profiles with the same $n_{e,ped}$ were obtained, as illustrated in Fig. 3. In these profiles, the width parameters, as measured from the LCFS to the inner part of the density barrier where profile flattening starts to occur, are very similar, as predicted by Eq. (5). The major difference between the two profiles is that the LCFS density for the L–mode profile is significantly higher than for the H–mode discharge. This feature is consistent with the model, as discussed in Section 3.3, and can be understood as a result of higher transport in the L–mode. This effect has been successfully modeled, as shown in Fig. 3(b), by producing two model profiles with identical parameters except that D_c and D_s were increased by an order of magnitude for one of the profiles. These model profiles show the same features as seen in the experimental data: the widths inside the LCFS are nearly identical and the LCFS density is higher for the profile with higher transport. Although these profiles are similar, there is an important difference in the dynamics. The particle flux (neutral density) was an order of magnitude higher for the profile with high diffusion coefficient than for the profile with low diffusion coefficient, a difference which was reflected in the experiment by the necessity to provide much more fueling for the L-mode discharge than the H–mode discharge.

The model also provides a simple explanation for the change in density profile that is normally observed at the L-H transition. As illustrated in Fig. 4, data from a typical discharge shows that by 50 ms after the transition, the pedestal density for the H–mode profile is significantly higher than in the L–mode case. Moreover, the H–mode density step has a narrower width and a steeper gradient than the L–mode profile. These trends are exactly what is predicted by the analytic model under the assumption that the core diffusion coefficient decreased at the L-H transition with the fueling rate remaining approximately constant.

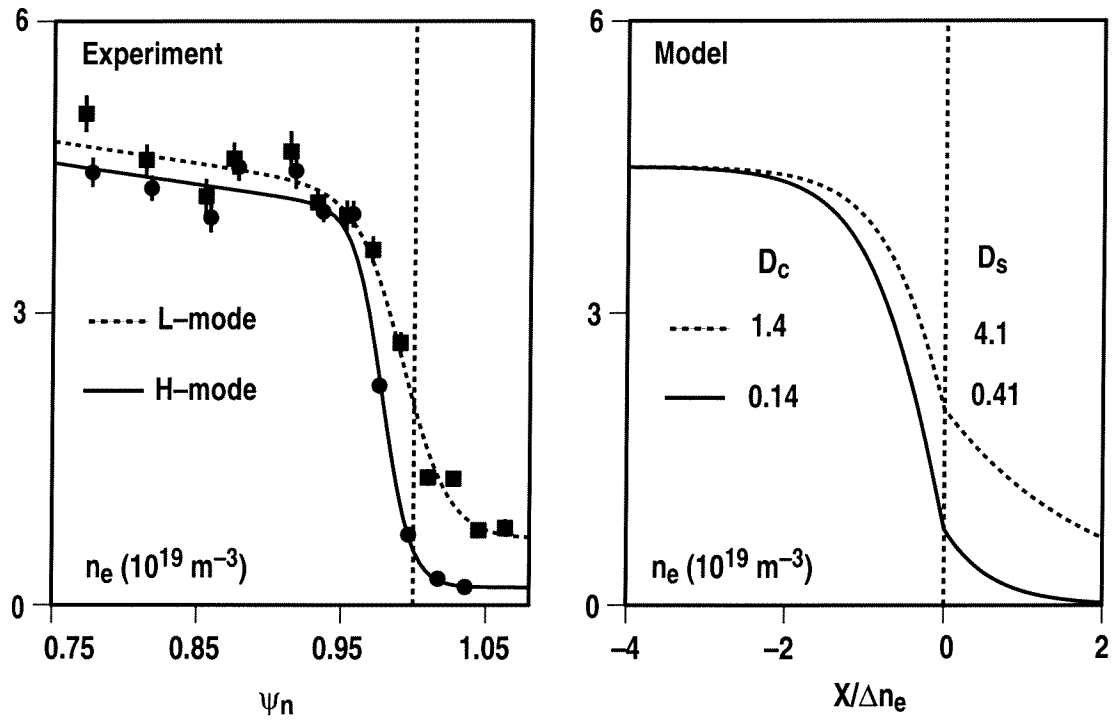

Fig. 3. Comparison of L–mode and H–mode density profiles with same pedestal density. (a) Experimental L–mode (squares plus dashed line) and H–mode (circles plus solid line) profiles shown as functions of poloidal flux. (b) Density profiles computed from model and plotted versus normalized physical distance. Model parameters for dashed curve are same as for solid curve except that D_S and D_C are increased by 10 times.

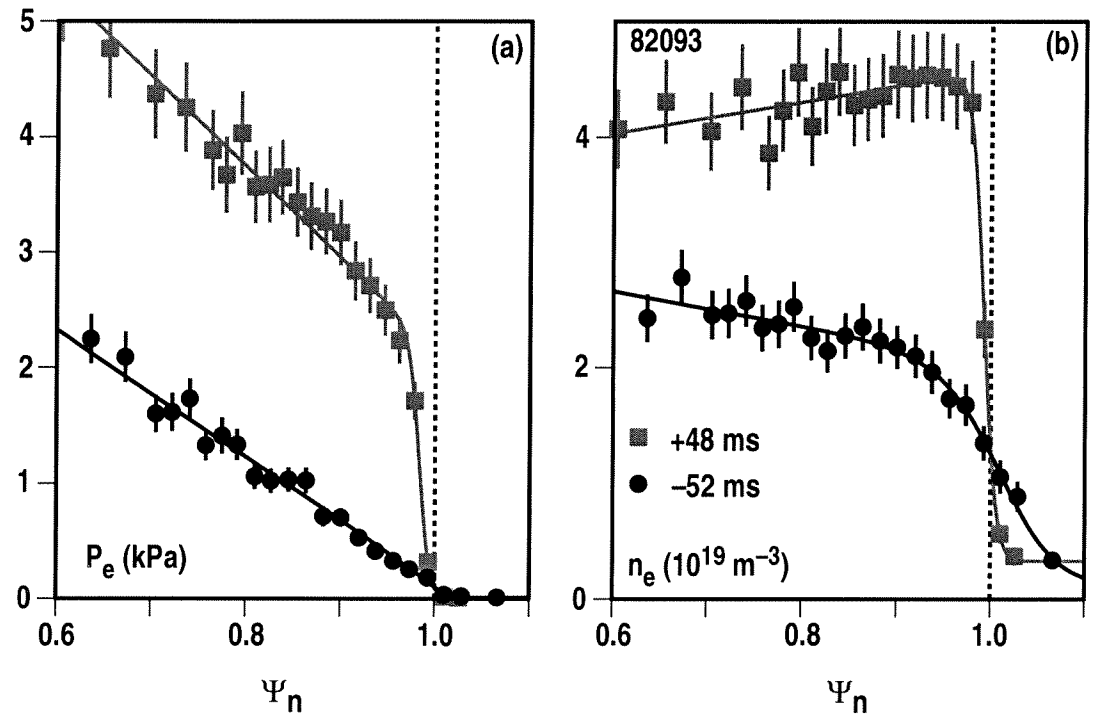

Fig. 4. Comparison of L–mode and H–mode profiles from ± 50 ms relative to an L-H transition. (a) Pedestal exists in electron pressure in H–mode but not in L–mode; (b) Relative to L–mode density profile, H–mode density profile has higher pedestal density, higher gradient and narrower width.

3.5. Benchmarking of analytic model

One potential objection to the analytic model is that it over-simplifies the complex fueling process to such a degree that the model is of little use. This objection has been addressed [18] with benchmarking of results of the analytic model to results from the sophisticated edge-modeling code UEDGE, and the comparison shows that the analytic model is in reasonable agreement with UEDGE. The UEDGE code is a 2-D fluid code that solves the plasma transport equations at the very edge of the core plasma and on the open field lines in the actual geometry of the non-circular DIII–D plasmas. UEDGE contains a fluid neutrals model which follows neutrals from their release at the divertor plates and walls of the vacuum vessel to the point of absorption in the plasma. Only charge-exchange neutrals are included in the present version of the model. In addition, UEDGE models fueling due to carbon impurities, an electron source that is small for the modeling performed here. The plasma transport is modeled by specifying the transport coefficients a priori.

In the comparisons that were performed, the pedestal density was varied in the UEDGE code with an appropriate particle source, adjusted so that net particle flux at the inner edge of the density pedestal was zero. The code was run with fixed particle diffusion coefficient, fixed thermal diffusivity and fixed heating power for all cases. For $n_{e,ped}$ varying in the range $4-7.5\times10^{19}m^{-3}$, the separatrix T_i was in the range 0.15–0.6 keV and the flux expansion factor was in the range 5–6. Density profiles were calculated from the analytic model with the same diffusion coefficient as used in UEDGE, with the separatrix T_i fixed at 0.15 keV and the flux expansion factor fixed at 5.2. The resulting density profiles from the UEDGE and analytic models show quite similar shapes and both exhibit a steepening of the profile as $n_{e,ped}$ increased [18]. Quantitative tests were also be performed by fitting the tanhfit function to these profiles to obtain width parameters For $n_{e,ped} \geq 4.5\times10^{19}$ m^{-3}, the widths from the two calculations agree within 10%–20% and the maximum gradients agree within ~ 20%–50% [18]. The larger differences between the two models for the gradients than for the widths indicates that the physics differences between the models show up as the profiles are examined in higher order detail. The comparison of the gradients is quite good, given that the gradients vary by over a magnitude in the experiment. The agreement between the two models starts to diverge somewhat for $n_{e,ped} \leq 4.5\times10^{19}m^{-3}$. This is understood as due to the importance of Frank-Condon neutrals, ignored by UEDGE, for these lower densities. In summary, the comparison between the two models is good in the range where good agreement is expected and these results support the use of the analytic model for studying the systematics of the edge electron density profile.

The analytic model predicts little dependence of the density width on temperature so long as the ratio of edge ion to electron temperatures remains roughly constant. Modelling with the

UEDGE code supports this conclusion, as illustrated in Fig. 5. The edge temperatures were varied in the code by an increase in the heating power with other parameters, including the pedestal density, remaining fixed. While varying over a factor of about two, the separatrix ion and electron temperatures maintained approximately the same ratio and the width of the computed density profile showed very little variation. The maximum density gradient decreased modestly as the temperature was increased. This was caused by a moderate increase of density at the separatrix, an effect that is possibly due to neutral transport physics in the SOL.

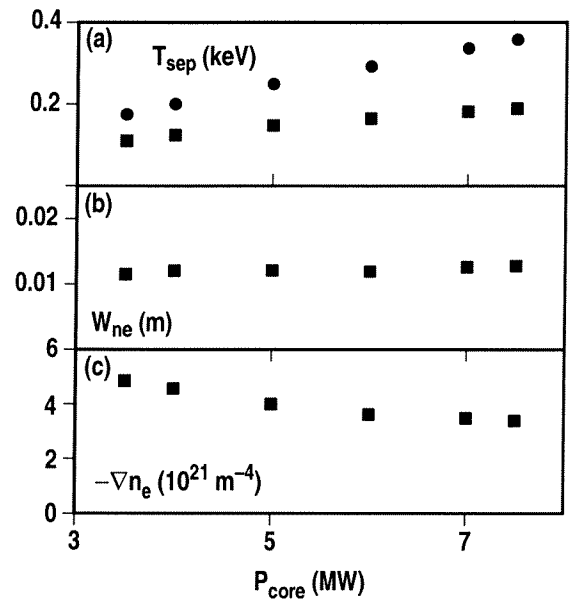

Fig. 5. Variation of edge parameters as function of power flowing from core in UEDGE calculations, with diffusivity and pedestal density held constant. (a) Separatrix temperature — Circles are ion data and squares are electron data; (b) Width of edge density profile (from tanhfit analysis of UEDGE profiles); (c) maximum density gradient at edge.

3.6. Effect of barrier in diffusion coefficient

One assumption used to produce a tractable model is that the diffusion coefficient is spatially uniform inside the LCFS with the possiblility of a step in D at the LCFS. Due to this assumption, the solution for the density profile shows that the width (inside the LCFS) is independent of diffusion for a given value of pedestal density. For the more realistic case that D_c varies in space, it is likely that the width will vary with diffusion, even for a given $n_{e,ped}$. A more realistic diffusion profile might be a square-well structure just inside the LCFS, which would emulate a transport barrier. Model calculations have been performed to examine the effects of such a diffusion profile [19]. These calculations are based on coupled continuity equations for neutrals and main ions, much as used here, except that the equations are solved numerically so that arbitrary diffusivity profiles can be employed. Results from these calculations show that when the width of the diffusivity barrier is wider then the ionization length, the barrier does not have much effect on the shape of the edge density profile. However, as the width of the barrier becomes smaller than the ionization length, effects are seen in the density profile with the width decreasing and the gradient increasing. However, a more important factor in controlling the maximum density gradient is the change in the diffusivity across the LCFS [19]. Except perhaps for extreme assumptions about the diffusivity profile, the details of the diffusion profile become less important for positions further into the plasma and away from the LCFS.

With the use of a barrier (square wall) in the diffusivity, the trends in the width and maximum gradient are quite similar to those obtained for a constant diffusivity, as illustrated in Fig. 6. For these data, the barrier in diffusivity was taken as 1 cm wide and the ratio of maximum to minimum diffusivity was set to four. A width parameter L_{ped} was defined as the pedestal density divided by the maximum density gradient. Figure 6(b) shows that this width parameter decreases with increasing pedestal density and is smaller for the barrier in diffusivity as opposed to constant diffusivity. The differences in the widths for the two diffusivity assumptions are large at low densities but moderate for the range of H–mode densities studied in the experiment. Figure 6(a) shows that the maximum gradient increases with pedestal density for the case with a barrier in the diffusivity and that the value of the gradient is within roughly a factor of two for the case with constant diffusivity. These results show that the details of the diffusivity profile affect the resulting density profile but do not significantly modify the trends and conclusions obtained from the basic analytic model. Moreover, as will be discussed in Section 4, the experimental evidence indicates that the transport barrier is as wide as or wider than the fueling depth. In that regime, the effect of the transport barrier width on the density step is not expected to be large. The change in the transport at the LCFS is predicted by the numerical modeling to have an important effect on the density profile.

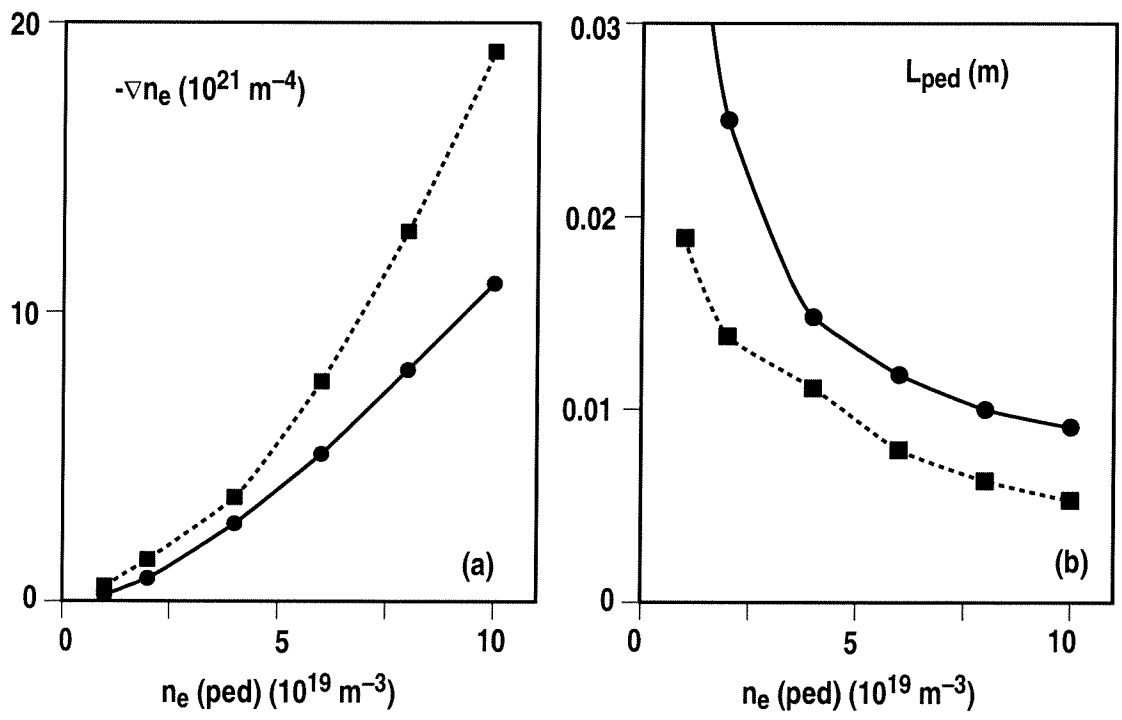

Fig. 6. Effect of barrier in diffusivity vs constant diffusivity. Barrier is 0.01 m wide and abuts the LCFS and ratio of maximum to minimum diffusivity is 4. (a) Maximum density gradient for barrier in diffusivity (squares) is ~50% larger than for constant diffusivity (circles). (b) Characteristic barrier width, equal to pedestal density divided by gradient, is ~50% larger for constant diffusivity (circles) than for barrier in diffusivity (squares).

3.7. Limitation of model at high edge temperatures

An important limitation to the model has been observed under some experimental conditions. Discharges have been produced in which the experimental values for the density width increase during the ELM-free phase even though $n_{e,ped}$ increases substantially during the same time [10]. This trend is opposite to that discussed throughout this paper. This phenomenon is correlated with high and rising pedestal temperatures, with both the ion and electron pedestal temperatures being above 500 eV. Thus, the reason that the model does not predict this behavior may well be related to inadequate treatment of temperature effects for temperatures above several hundred electron volts. In that temperature range, the rate of ionization slowly decreases and the rate of charge exchange increases as temperature is increased. Thus, neutral transport due to multiple charge exchange effects may be an important process and would give deeper penetration of the neutrals than is accommodated in the model. This process has not yet been examined with detailed modeling.

4. COMPARISON OF TRANSPORT BARRIER WIDTH AND DENSITY WIDTH

The previous discussion strongly indicates that the width of the density step, the region of steep gradient in the density, is primarily a measure of the fueling depth. Thus, it cannot necessarily be concluded that the width of the density step is a measure of the width of the transport barrier. On the other hand, the Hinton-Staebler model predicts that the width of the transport barrier should be comparable to the fueling depth. Experimental data are used here to test this prediction, and the analysis is consistent with this prediction.

The width of the electron temperature barrier, as measured with fits of the *tanh* function, is used as a measure of the width of the transport barrier. The outer edge of the temperature barrier is generally taken as a good measure of the locations of the LCFS and thus this width will be called Δ_{Te}. For this comparison, it is necessary to have an estimate of the density width Δ_{ne} that is inside the LCFS. This estimate is obtained by measuring the distance between the outer edge of the electron temperature barrier to the inner edge of the density step. Given these assumptions, Fig. 7 shows examples of temperature barriers which are comparable in width to the density step [Fig. 7(a)] and wider than the density step [Fig. 7(b)]. Figure 7 also shows that an alternate measure of transport, the quantity $\left(n_e \nabla T_e\right)^{-1}$, suggests that the transport barrier is somewhat

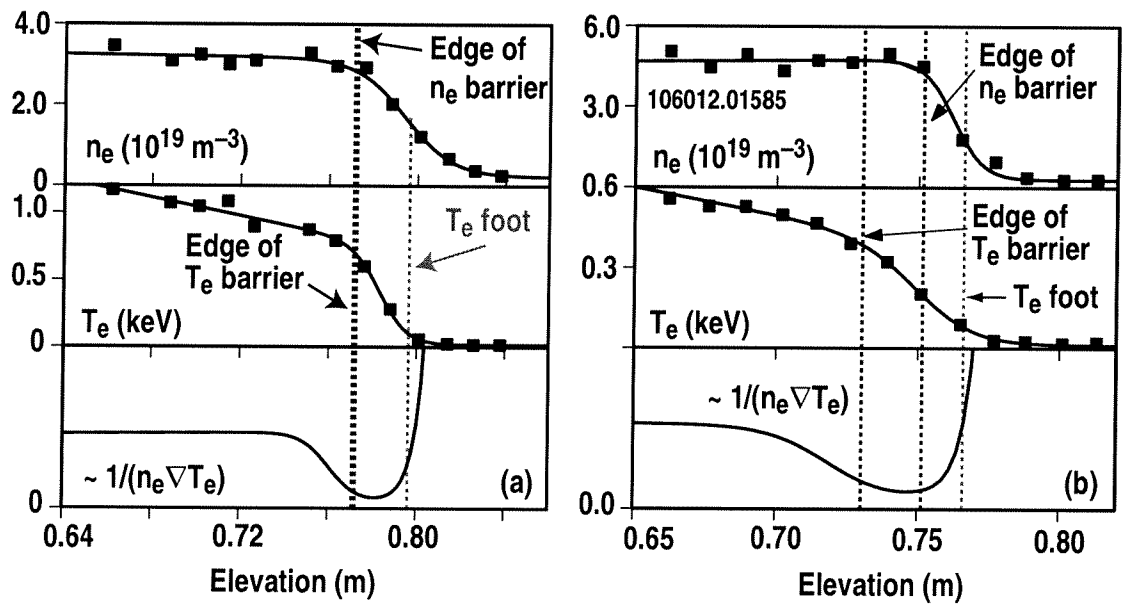

Fig. 7. Comparison of transport barrier width, as indicated by barrier in electron temperature with fueling depth, as indicated by step in electron density. Also shown is estimate of transport coefficient. (a) Case with width of T_e barrier being about equal to width of n_e step; (b) Case with width of T_e barrier being larger than width of n_e step.

wider than given by width Δ_{Te} from the *tanh* analysis. Thus, the width parameter Δ_{Te} appears to be a conservative measure of the width of the transport barrier.

The profiles in Fig. 7 are typical examples of edge profiles in DIII–D and suggest that the transport barrier extends as far as or further than the density step into the plasma. A more comprehensive picture is obtained by plotting a histogram of the number of occurrences of various values of the ratio of Δ_{Te}/Δ_{ne} for a large data set, as shown in Fig. 8. The data for Fig. 8 are the H–mode data used in Figs. 1 and 2; averaging has not been performed in Fig. 8, so many more data points are available than for Figs. 1 and 2. For each bin of the quantity Δ_{Te}/Δ_{ne}, the histogram shows the number of times the ratio was found to be in that bin. The histogram shows clearly that Δ_{Te} is almost always between 1 and 2 times Δ_{ne} with the most probable value being about 1.1–1.2 times Δ_{ne}. The average value of the ratio is 1.3–1.5. There are very few data points with a ratio below one and these are within experimental error of being one. Thus, the data show that extent of the density step inside the LCFS forms a lower bound for the extent of the transport barrier; the transport barrier can extend up to another Δ_{ne} into the plasma.

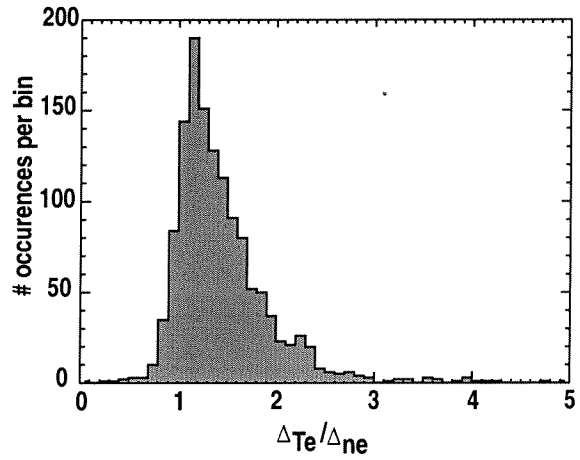

Fig. 8. Histogram showing number of occurrences of various ratios of electron temperature barrier width to electron density barrier width. Outer edge of density barrier is taken as outer edge of temperature barrier.

5. CONCLUSIONS AND DISCUSSION

The data and analysis presented here strongly indicate that the width of the steep gradient region in the edge H–mode density profile is approximately equal to the fueling depth, which is set self-consistently by the edge particle transport and neutral transport. With the fueling adjusted to produce a given pedestal density, the resulting width and maximum gradient of the density profile are weakly dependent on the magnitude of the transport, with the effect of transport showing up most prominently at the separatrix. These conclusions are based on the comparison of experimental widths and gradients of the density profile with predictions of an analytic model based on a self-consistent solution of the particle and neutral transport. These conclusions also follow from the fact that L–mode density profiles also have substantial gradients at the plasma edge, even though no transport barrier is known to exist. L–mode and H–mode profiles with the same pedestal density have very similar widths and gradients, as expected from the self-consistent model.

The H–mode profiles in DIII–D are also consistent with predictions of the Hinton-Staebler model that the width of the transport barrier is controlled primarily by the particle source. The evidence is that the most probable width of the electron temperature barrier is very nearly equal to the width of the density step inside the last closed flux surface. However, the transport barrier can extend up to two times the width of the density step, indicating that fueling provides a lower bound on the size of the transport barrier. In the context of the Hinton-Staebler model, the heat flux from the core may also be providing some control of the transport barrier.

An important implication of the theoretical model and the results presented here is that techniques to modify the particle fueling might provide means to control the width of the density step. In particular, a technique which provides deeper fueling than conventional gas-puffing might produce a density step, and therefore a transport barrier, which is wider than conventional H–mode barriers. This technique would require that recycling from material surfaces be eliminated as a significant source of fueling.

REFERENCES

[1] OSBORNE, T.H., et al., Proc. 24th Eur. Conf on Controlled Fusion and Plasma Physics, Berchtesgaden, Germany, 1997 (European Physical Society, Petit-Lancy, 1997), Vol 21A, p. 1101.

[2] GREENWALD, M, et al., Nucl. Fusion. **37,** (1997) 793.

[3] KINSEY, J.E., WALTZ, R.E. and SCHISSEL, D.P., Proc. 24th Eur. Conf on Controlled Fusion and Plasma Physics, Berchtesgaden, Germany, 1997 (European Physical Society, Petit-Lancy, 1997), Vol 21A, p. 1081.

[4] SNYDER, P.B., WILSON, H.R., FERRON, J.R. et al, Phys. Plasmas **9**, (2002) 2037.

[5] HINTON, F.L. and STAEBLER, G.M, Phys. Fluids B **5**, (1993) 1281.

[6] LEBEDEV, V.B. and DIAMOND, P.H., Phys. Plasmas **4**, (1997) 1087.

[7] WAGNER, F. and LACKNER, K., *Physics of Plasma-Wall Interactions in Controlled Fusion*, (edited by D.E. Post and R. Behrisch, published by Plenum Press, New York in cooperation with NATO Scientific Affairs Division), Series B, Physics Vol. 131, 931 (1986).

[8] ENGELHARDT, W. and FENENBERG, W., J. Nucl. Mater. **76-77**, (1978) 518.

[9] MAHDAVI, M.A., *et. al*, Nucl Fusion **42** (2002) 52.

[10] GROEBNER, R.J., *et al*, Phys. Plasmas **9**, (2002) 2134.

[11] GROEBNER, R.J., *et al*, Plasma Phys. Control Fusion **44**, (2002) A265.

[12] MAHDAVI, M.A., et al., 29th EPS Conference on Plasma Phys. and Contr. Fusion Montreux, 17-21 June 2002 ECA Vol. 26B, P-2.098 (2002).

[13] MAHDAVI, M.A., *et al*, "Consistency of the Divertor and Core Plasma Densities for Burning Plasmas", to be submitted for publication.

[14] YOKOMIZO, *et al,* Plasma Physics and Contr. Nuclear Fusion Research 1982, Vol III, IAEA, Vienna (1983) 173.

[15] ROGNLIEN, T.D., *et. al*, Contrib. Plasma Phys. **34**, (1994) 362.

[16] GROEBNER, R.J. and OSBORNE, T.H., Phys. Plasmas **5**, (1998) 1800.

[17] CARLSTROM, T.N., et al., Rev. Sci. Instrum. **63**, (1992) 4901.

[18] WOLF, N.S., et al., Proc. of 15th Int. Conf. on Plasma Surface Interactions, Gifu, 2002, to be published in J. Nucl. Mater.

[19] STANGEBY, P.C., "On the relative role of neutral and plasma transport in the formation of the density pedestal in magnetically confined plasmas", to be submitted for publication.

ACKNOWLEDGMENTS

The authors gratefully acknowledge the assistance of the entire DIII–D staff in obtaining these results and express their appreciation to T. Taylor and R. Stambaugh in supporting this work. Work supported by U.S. Department of Energy under Contracts DE-AC03-99ER54463, W-7405-ENG-48, DE-0AC05-00OR22725, SC-G903402, and Grants DE-FG03-96ER54373, DE-FG03-01ER54615 and DE-FG03-95ER-54294.